BiFeO 3 Nanoparticles: The "Holy-Grail" of Piezo-Photocatalysts?

Wafa Amdouni, Matthieu Fricaudet, Mojca Otoničar, Vincent Garcia, Stephane Fusil, Jens Kreisel, Hager Maghraoui-Meherzi, Brahim Dkhil

$BiFeO_3$ Nanoparticles: The "Holy-Grail" of Piezo-photo-catalysts?

Wafa Amdouni, Matthieu Fricaudet, Mojca Otoničar, Vincent Garcia, Stephane Fusil, Jens Kreisel, Hager Maghraoui-Meherzi, and Brahim Dkhil**

Dr. W. Amdouni, Prof. H. Maghraoui-Meherzi
Université de Tunis El-Manar, Faculté des Sciences de Tunis, Laboratoire de Chimie Analytique et Électrochimie LR99ES15, Campus Universitaire de Tunis El-Manar, 2092 Tunis, Tunisie
E-mail: wafa.amdouni@fst.utm.tn

Dr. W. Amdouni, M. Fricaudet, Prof. B. Dkhil
Université Paris-Saclay, CentraleSupélec, Laboratoire Structures, Propriétés et Modélisation des Solides, UMR CNRS 8580, 91190 Gif-sur-Yvette, France
E-mail: brahim.dkhil@centralesupelec.fr

Dr. M. Otoničar
Jožef Stefan Institute and Jožef Stefan Postgraduate School, Jamova 39, 1000, Ljubljana, Slovenia

Dr. V. Garcia, Dr. S. Fusil
Unité Mixte de Physique, CNRS, Thales, Université Paris-Saclay, Palaiseau 91167, France

Prof. J. Kreisel
Department of Physics and Materials Science, University of Luxembourg, and Materials Research and Technology Department, Luxembourg Institute of Science and Technology, L-4422 Belvaux, Luxembourg

Keywords: $BiFeO_3$, piezocatalysis, piezo-photocatalysis, $BiFeO_3$/P(VDF-TrFE)

Abstract

Recently, piezoelectric-based catalysis has been demonstrated to be an efficient means and promising alternative to sunlight-driven photocatalysis, where mechanical vibrations trigger redox reactions. Here, we show that 60 nm average size $BiFeO_3$ nanoparticles are very effective for piezo-degrading Rhodamine B (RhB) model dye with record degradation rate values reaching 13810 L mol^{-1} min^{-1}, and even 41750 L mol^{-1} min^{-1} (i.e., 100% RhB degradation within 5 min) when piezocatalysis is synergistically combined with sunlight photocatalysis. We also demonstrate that these $BiFeO_3$ piezocatalytic nanoparticles are versatile towards several cationic and anionic dyes, and pharmaceutical pollutants, with over 80% piezo-decomposition within 120 min among the six pollutants tested. The maintained high piezoelectric coefficient combined with low dielectric constant, high elastic modulus and the nanosized shape make these $BiFeO_3$ nanoparticles extremely efficient piezocatalysts. To avoid subsequent secondary pollution and enable their reusability, the $BiFeO_3$ nanoparticles are further embedded in a polymer P(VDF-TrFE) matrix. The as-designed free standing, flexible, chemically stable and recyclable nanocomposites still keep remarkable piezocatalytic and piezo-photocatalytic performances (i.e., 92% and 100% RhB degradation, respectively, within 20 min). This work opens a new research avenue for $BiFeO_3$ that is the model multiferroic material, and offers a new platform for water cleaning, as well as other applications such as water splitting, CO_2 reduction or surface purification.

1. Introduction

Water constitutes for every human being the major resource for its own living. However and despite their social benefits, the industrial and technological developments of modern societies have intensively exploited and polluted this precious resource for fulfilling larger production objectives at reduced costs in many fields, including not only industry but also agriculture, farming and transportation. Furthermore, the generalized use of chemicals, such as pharmaceutical drugs and other bio-inhibiting molecules, has caused the accumulation of pollutants in water, also affecting the equilibrium of ecosystems. It is therefore crucial to look for efficient routes to clean water from pollutants and hazardous molecules, by employing effective and environmentally friendly materials, combined with low energy consumption.

Photocatalysis using the free, abundant and inexhaustible solar source remains one of the most promising and energy saving processes, at minimum costs for converting sunlight energy into chemical energy in semiconductors.[1] However, challenges remain to improve the photochemical conversion efficiency and limit the recombination of photogenerated carriers during the catalytic process through doping,[2] heterojunction structure construction,[3] defect states,[4] and loading co-catalyst.[5]

In recent years, ferroelectric materials have received considerable attention as photocatalysts because of their spontaneous polarization (that is switchable under the application of an external electric field). In ferroelectrics, once the light excitation generates electron-hole pairs, the polarization acts like an internal electric field promoting the separation of photo-excited electrons (e^-) and holes (h^+) and thus increasing their lifetime by reducing their recombination.[6] Moreover, ferroelectrics are good piezoelectric materials, a property that allows the generation of electric charges by mechanical stress, or reversely, to the deformation under the application of an electric field, known as piezoelectricity. Although piezoelectricity has been widely exploited in pressure sensors,[7] actuators and transducers,[8] it has been only recently used to directly drive catalytic redox reactions; coined as piezocatalysis.

Piezocatalysis is indeed a new advanced oxidation process where mechanical vibration solicitations trigger polarization modulations. The latter produce a built-in electric field in the piezocatalyst, which in turn separates the e^- and h^+ making them available for redox reactions.[9] Several ferroelectrics have been demonstrated as efficient piezocatalysts for the degradation of organic pollutants and water splitting for hydrogen production (H_2) by applying external mechanical forces. These include classical ferroelectric-based materials such as $PbZr_xTi_{1-x}O_3$ (PZT),[10] $BaTiO_3$ (BTO),[11] $KNbO_3$ (KNO),[12] or $NaNbO_3$ (NNO),[13] as well as relaxor-based ferroelectrics like $Pb(Mg_{1/3}Nb_{2/3})O_3$-$xPbTiO_3$ (PMN-PT),[14] $Na_{0.5}Bi_{0.5}TiO_3$ (BNT),[15] or $Sr_{0.5}Ba_{0.5}Nb_2O_6$ (SBN).[16] These materials have been selected because of their strong piezoelectric coefficient. However, to efficiently produce electrical charges from a piezoelectric, as it is currently done in piezoelectric energy harvesters, the figure of merit (FOM)[17] which characterizes the performances of the piezoelectric harvester writes as $FOM \sim d^2.Y/\varepsilon$, where d is the piezoelectric coefficient, Y the Young elastic modulus and ε the static (low frequency) dielectric constant. This means that beyond the piezoelectric coefficient that should be indeed maximized, the dielectric response should be minimized, considering that the Young modulus for all the aforementioned inorganic oxides are similar (i.e., 130-230 GPa while it is only ~2 GPa in case of e.g., PVDF-based polymers). It is also worth reminding that the piezoelectric properties usually degrade when going towards nanoscale, and especially drop down below 100

nm-sizes.[18] However, these are typically the requested sizes for improving the catalytic activity because their surface-to-bulk ratio increases and the detrimental recombination rate decreases, allowing more charge carriers to reach the surface and become available for initiating redox reactions. On the other hand, bismuth ferrite ($BiFeO_3$-BFO), is characterized by a large polarization of ~100 μC cm^{-2} (along the [111] polar axis), a piezoelectric coefficient (d_{33}) of ~100 pm V^{-1},[19] and dielectric constant of ~55,[20] and is often coined as the "holy-grail" multiferroic compound because of the coexistence of both polarization and magnetization at room temperature. With its high piezoelectric response and low enough dielectric response, BFO could be a highly suitable compound for piezocatalytic activity, as suggested very recently in either BFO nanosheets and nanowires or core-shell structures with BFO particles of 100-500 nm sizes.[21]

Moreover, the small band gap (~ 2.2-2.6 eV)[22] compared to other ferroelectrics (>3 eV), has made this model multiferroic suitable for photocatalytic applications using wider illumination range freely available in natural sunlight.[23] Note also that the typical photocarriers diffusion length is lower than 100 nm which imposes a maximal size to limit their recombination.[22]

In this work, we show that 60 nm-sized BFO nanoparticles (NPs) display extremely high piezocatalytic activity efficiency, with record value, as well as wide versatility enabling to piezo-decompose various organic contaminants such as dyes and pharmaceuticals, when subjected to ultrasonic wave excitation in the dark without the involvement of any sacrificial molecules or cocatalysts. Interestingly, combined with light illumination, BFO is found for the first time to have a much higher piezocatalytic efficiency, as the catalytic activity dramatically improves allowing the degradation rate of the model Rhodamine B (RhB) dye to reach 41750 L mol^{-1} min^{-1} (i.e., ~ 100% degradation ratio within 5 min) via this piezo-photocatalysis process. This synergistic piezo-photocatalysis using BFO nanoparticles is the fastest degradation rate ever reported. Such remarkable efficiency is attributed to the nanosize of the particles reducing the recombination process, and the maintained high piezoelectric response. Moreover, although the high catalytic efficiencies are mostly achieved by dispersing the particulate-based catalyst in the solution of organic pollutants, which ensures a large contact area for catalytic reactions, catalyst particles are difficult to be collected and reused. Thus, they tend to diffuse and cause secondary pollution in water bodies, which greatly restrict their applicability in practical wastewater treatment. We therefore used poly(vinylidenefluoride-trifluoroethylene) [P(VDF-TrFE)] ferroelectric copolymers as a matrix to embed the BFO NPs, taking advantage of its chemical inertness and high flexibility nature, for designing, for the first time, $BiFeO_3$/P(VDF-

TrFE) composite films as free-standing, non-toxic, stable and reusable catalyst systems. We show they largely conserve their high piezo-photocatalytic efficiency. Such bio-compatible and non-toxic composites may provide an easily applicable platform for large scale applications in wastewater treatment via utilizing both solar energy and environmental mechanical energies.

2. Results and Discussions

2.1. Micro-structural and Piezoelectric Characterization

$BiFeO_3$ NPs were first successfully synthesized via a facile chemical bath method and post-annealed at 500°C in air environment, for crystallization. **Figure 1**a shows the X-ray diffraction (XRD) pattern exhibiting a high phase purity without any parasitic phases and all Bragg peaks well-matching with the JCPDS card no. 86-1518, corresponding to the perovskite structure of BFO with rhombohedral R3c symmetry. Rietveld refinement was used to determine the unit cell parameters which are found to be a = 5.580 Å, c = 13.877 Å and V = 374.26 $Å^3$,[23] values that are comparable to those of the bulk, suggesting the piezoelectric response should be conserved despite the nanosize of the BFO particles. The transmission electron microscopy (TEM) analysis of the BFO NPs is presented in the inset of Figure 1a. The shape of the NPs is semi-hexagonal to spherical with an average size of about 60 nm (Figure S1, Supporting Information). In agreement with the well-defined Bragg peaks (Figure 1a), the synthesized NPs are also highly crystalline in nature as evidenced from the high-resolution TEM image exhibiting well-resolved lattice fringes (right inset of Figure 1a).

To tackle the issues related to collecting the catalyst particles, we then fabricated a composite film where 5 % of BFO NPs were embedded into a P(VDF-TrFE) (75-25) copolymer using a simple scalable tape casting method (see Experimental Section). Figure 1b shows scanning electron microscopy (SEM) images displaying the surface and cross-section morphology of the 25 µm thick BFO/P(VDF-TrFE) flexible composite, showing the uniform distribution of BFO fillers throughout the polymer matrix. The pure P(VDF-TrFE) had a morphology of intertwined needle-like structure (Figure S2a, Supporting Information). From Figure S2b of the Supporting Information, it is clear that the characteristic peaks for rhombohedral BFO and P(VDF-TrFE) copolymer could be identified. The peak at 20.26° is associated with the (110) and (200) diffraction of the β-phase of P(VDF-TrFE), suggesting that that the crystalline phase of the polymer matrix in the composite is mainly β-phase, and the structure does not change upon addition of BFO, which is also confirmed by Raman spectroscopy (Figure S3, Supporting

Information) . Note that the BFO/P(VDF-TrFE) composite films could be prepared also on a larger area (inset Figure S2b), and is highly flexible (Figure 1b$_1$).

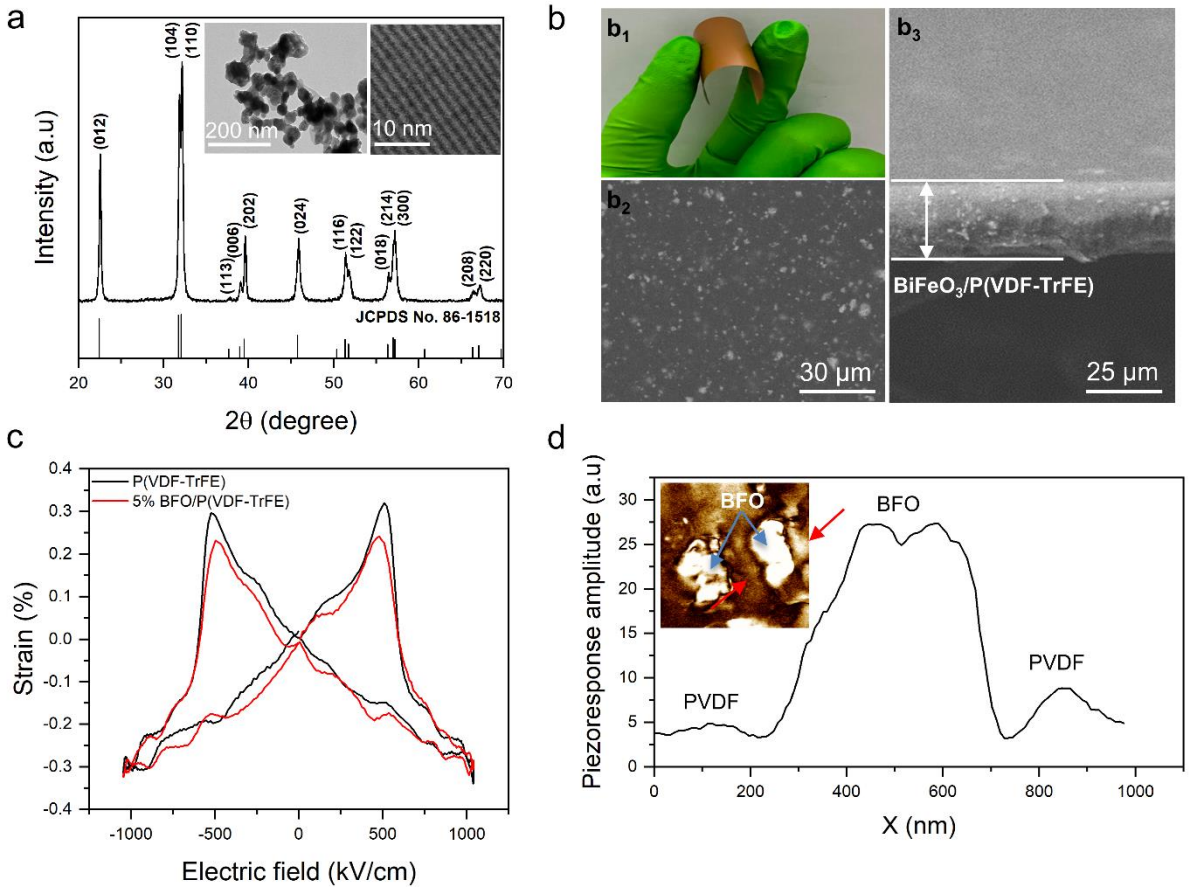

Figure 1. Microstructural and piezoelectric characterizations of $BiFeO_3$. a) XRD pattern of BFO nanoparticles and the inset images showing their corresponding TEM and high-resolution TEM images. b) Surface morphology of fabricated BFO/P(VDF-TrFE) composite film: (b_1) photograph of the BFO/P(VDF-TrFE) device demonstrating the flexibility by finger pressing. (b_2) SEM image of BFO/P(VDF-TrFE) and (b_3) cross-sectional SEM image of BFO/P(VDF-TrFE). c) Strain versus electric field of the BFO/P(VDF-TrFE) composite as well as the reference P(VDF-TrFE). d) Profile of the piezoresponse across a BFO bundle extracted from the out-of-plane PFM amplitude image displayed in inset (between the two red arrows). The bright contrast observed on the $BiFeO_3$ particles corresponds to a polarisation pointing downward. The black contrast of the P(VDF-TrFE) matrix also corresponds to downward polarisation (P(VDF-TrFE) and $BiFeO_3$ have opposite signs for respective piezoresponse, leading to phase contrast inversion).

The piezoelectric properties of BFO NPs were determined by combining studies on a macroscopic and nanoscopic scale. While PFM can be an alternative approach for evaluating the piezoelectric and ferroelectric properties of the material at the nanoscale, it does not provide quantitative insights and is challenging for nano-objects which can move under the action of

the scanning PFM tip. To find out the piezoelectric properties of our NPs, we therefore start measuring the macroscopic response on the BFO/P(VDF-TrFE) composites. The macroscopic piezoelectric strain versus electric field responses of the as-designed composite and pure P(VDF-TrFE) are displayed in Figure 1c, and show a reversed (negative piezoelectric coefficient) "butterfly-like" loop typical for PVDF-based polymers. Both loops are very similar, indicating that the addition of 5% BFO NPs only weakly, if any, contribute to the macroscopic piezoelectric response of the composite. The effective macroscopic piezoelectric coefficient *d* is determined from the derivative of the strain with respect to the field at strain zero and is found to be d = -16 pm V^{-1}, which corresponds to the value of pure P(VDF-TrFE) copolymer.[24] This macroscopic measurement allows us to have an absolute value of P(VDF-TrFE) that we will use to extract the response of the BFO by local PFM measurement. Local PFM measurements are depicted in Figure 1d. The topography and both vertical and lateral piezoresponse (amplitude and phase) experiments were conducted and show piezoelectric activity on both the BFO single particles and the P(VDF-TrFE) matrix (Figure S4, Supporting Information). Nevertheless, measuring the piezoresponse on isolated NPs is difficult because the NPs signal is perturbed by the neighboring polymer response and convoluted with that of the PFM tip (few tens of nm thus comparable to the NP size) (Figure S4e-f, Supporting Information). The inset of Figure 1d shows the PFM phase contrast of two sub-micron agglomerates of BFO NPs embedded in the P(VDF-TrFE) matrix. The typical amplitude of the signal measured across such agglomerates is shown in Figure 1d and exhibits an about four times higher response for BFO compared to the P(VDF-TrFE) alone. While the PFM amplitude is directly related to the piezoelectric coefficient, such measurements cannot provide absolute piezoelectric values. Nevertheless, combining our macroscopic measurements (Figure 1c) that provides the absolute piezoelectric coefficient value of P(VDF-TrFE) is $|d|$ = 16 pm V^{-1} and the aforementioned PFM data, the effective piezoelectric coefficient of our BFO NPs is likely to be about 4 times higher i.e., 64 ±10 pm V^{-1}, which is comparable to bulk values reported in the literature.[25] Thus, despite their nanosize and in contrast to many other ferroelectrics where the piezoelectric coefficient significantly drops down,[18a, 18c, 18d, 26] with decreasing size, our BFO NPs keep their good piezoelectric properties.

2.2. Highly Efficient and Versatile $BiFeO_3$ Nano-Piezocatalysts

Now that we have shown the piezoelectric properties of our 60 nm size BFO NPs are conserved, let us study their efficiency for removing pollutants from water by the piezocatalytic effect. For this goal, their capability to initiate the mechanical-to-chemical energy conversion

under the application of ultrasonic vibrations is investigated through the degradation of a model aqueous organic dye pollutant that is Rhodamine B (RhB), which is often considered in the literature for testing. Our experiment design is illustrated in Figure S5 (Supporting Information) and described in the experimental part. The ultrasonic wave constantly applied on the liquid produces numerous cavitation bubbles, and in turn, large and periodic mechanical stresses are induced and generate piezoelectricity on the dispersed BFO NPs. The original pink color solution fades and becomes transparent after 30 min as shown in the inset of **Figure 2**a. To investigate the degradation process, aliquots (~3 mL) were sampled at specific intervals and analyzed by UV-Vis spectroscopy. The degradation curves C/C_0 are displayed in Figure 2a, where C and C_0 are the concentrations of RhB at time = t and t = 0, respectively. From the figure, one can observe that there is no degradation of RhB in the absence of either ultrasonic vibrations or BFO nanocatalysts (in dark condition). In contrast, an ultra-high degradation activity was observed as the ultrasonic wave is introduced to propagate in the RhB solution, when using BFO NPs under the dark condition. The RhB degradation ratio is 93% within 10 min and reaches 97% after 30 min of ultrasonic vibrations. Using pseudo-first-order reaction through Equation (1):

$$\ln\left(\frac{C_0}{C}\right) = k_{\text{obs}}t \qquad (1)$$

The observed rate constant (k_{obs}) is found to be 0.1381 min^{-1} (Figure S6, Supporting Information) which is, to the best of our knowledge, the highest ever reported value (see Table S1, Supporting Information). Indeed, this value is almost 46 and 13 times higher than that of previously reported perovskite-based ferroelectric i.e., $KNbO_3$ (k_{obs} = 0.003 min^{-1}) and $BaTiO_3$ (k_{obs} = 0.01 min^{-1}),[12, 27] 66 and 9 times higher than that of ferroelectric heterostructures $Bi_{0.5}Na_{0.5}TiO_3$@TiO_2 (k_{obs} = 0.0012 min^{-1}) and ZnO/$BaTiO_3$ (k_{obs}= 0.0153 min^{-1}),[15, 28] and 5.5 times than that of ferroelectric $Bi_4Ti_3O_{12}$ (k_{obs} = 0.0252 min^{-1}) with Aurivillius structure.[29] To our knowledge, this value is also much higher than that of 150 nm-thick BFO (edge length 2-3 mm) nanosheets (k_{obs} = 0.0143 min^{-1}), (30 mm long) nanowires (k_{obs} = 0.0431 min^{-1}), and core-shell $CoFe_2O_4$@BFO nanostructures (k_{obs} = 0.050 min^{-1});[21a, 21d] (see Table S1, Supporting Information; **Figure 4**). Nevertheless, these recently reported values support our findings showing that BFO material is an excellent piezocatalyst. Moreover, as our degradation rate value is about 3 to 9 times much higher than in bigger BFO nanostructures,[21a, 21d] they also strongly suggest that the nanosize of our BFO NPs is much more appropriate for getting improved piezocatalytic activity, probably because the recombination rate in such NPs is much lower.

The piezocatalytic mechanism is schematically shown in Figure 2b. While this mechanism is not fully clear yet, it is attributed to the stress-induced piezoelectric potential or piezopotential (i.e., built-in electric field), which is generated by the fluctuating mechanical forces created by the sporadic collapse of the acoustic cavitation walls of bubbles in the solution. In turn, this "jerky" piezopotential will separate the electrons (e^-) and holes (h^+) that are thermally generated and drive them to the surface of the particle (see Figure S7, Supporting Information). Once these free e^- and h^+ reach the surface, they can therefore interact with solution molecules. The individual chemical reaction of the piezocatalytic process can be expressed as follows:

$$BFO \xrightarrow{vibration} BFO + e^- + h^+ \quad (2)$$

$$e^- + O_2 \rightarrow \bullet O_2^- \quad (3)$$

$$h^+ + OH^- \rightarrow \bullet OH \quad (4)$$

$$RhB\ dye\ molecules + \bullet O_2^- + \bullet OH \rightarrow degradation\ products \quad (5)$$

To confirm the above-proposed mechanism, where •OH and $\bullet O_2^-$ radicals are active species for the organic dye degradation in the dark, radical-trapping experiments were performed by introducing disodium ethylene diamine tetra-acetate dehydrate (EDTA-2Na), tert-butyl alcohol (TBA), and benzoquinone (BQ) additives as scavengers for holes (h^+), hydroxyl radicals (•OH), and superoxide radicals ($\bullet O_2^-$), respectively, into the piezocatalytic reaction system. As shown in Figure 2c and Figure S8 of the Supporting Information, the piezocatalytic effect was remarkably restrained by the addition of TBA or BQ, indicating that both •OH and $\bullet O_2^-$ radicals are of importance during the piezocatalytic degradation reaction. Meanwhile, after adding the hole scavenger EDTA, the RhB aqueous solution continues to maintain an effective degradation performance, indicating that h^+ are less important for piezocatalysis. These results imply that •OH and $\bullet O_2^-$ are the main active species responsible for piezocatalytic degradation of RhB using BFO NPs, in agreement with the proposed mechanism in Figure 2b.

To show the piezocatalytic versatility of BFO NPs and go beyond RhB, methylene blue (MB; cationic dye), methyl orange (MO; anionic dye), indigo carmine (IC; anionic dye), tetracycline (TC; antibiotic drug), and carbamazepine (CBZ; persistent and toxic drug) were selected to probe the breadth of BFO piezocatalytic activity. As shown in Figure 2d, near complete piezo-degradation was achieved for all pollutants with over 80% efficiency (see also Figure S9 and Figure S10a, Supporting Information). The corresponding observed rate constant of our BFO (Figure S10b, Supporting Information) and other piezocatalysts reported in the literature are provided in Table S2 of the Supporting Information. By comparing the rate constant, catalyst dosage and organic pollutant concentration, it could be found that the

piezocatalytic performance of BFO nanocatalysts prepared in this study for the degradation of MB, MO, IC, TC and CBZ was obviously higher than all the other previously reported piezoelectric catalysts. This finding highlights the potential of BFO nanoparticles for wastewater treatment through mechanical energy without any additional energy input, bearing in mind that such energy can be available at any time of the day and anywhere, in contrast to intermittent sunlight.

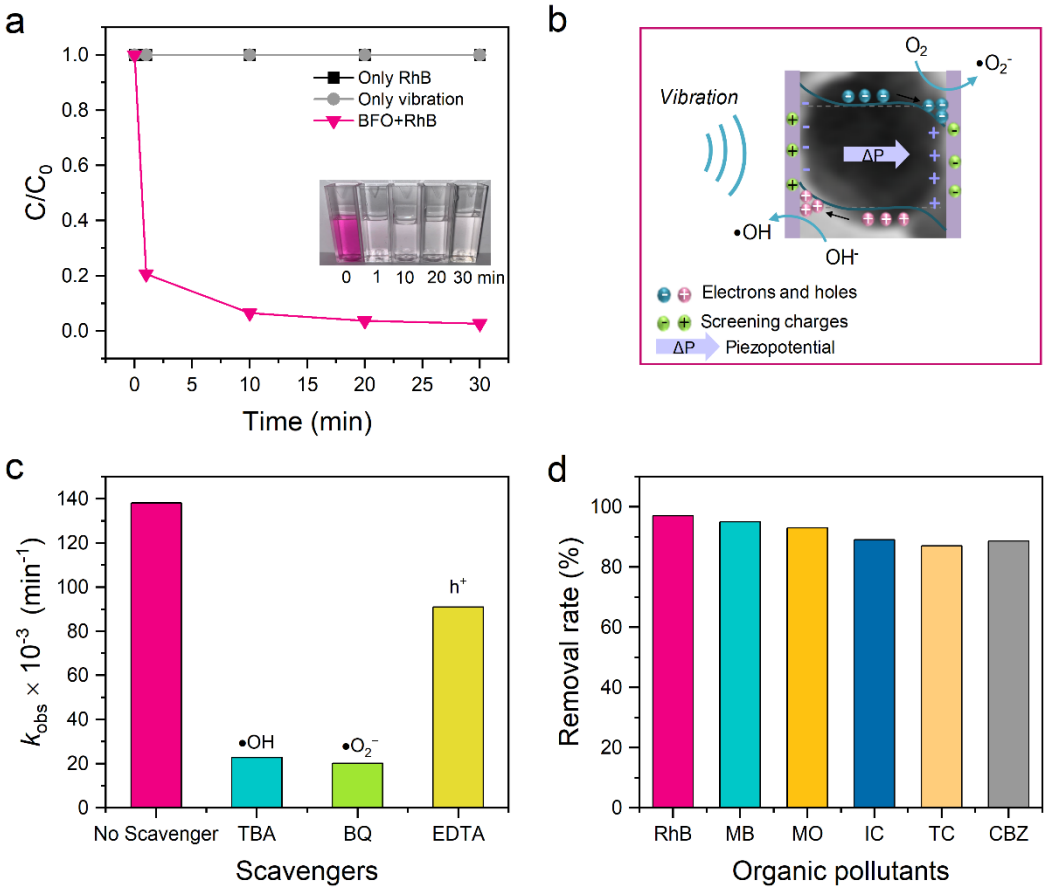

Figure 2. Piezocatalytic performance of $BiFeO_3$ nanoparticles. a) Degradation efficiency of RhB using BFO nanoparticles in the dark under ultrasonic wave (100 W, 45 kHz). The inset is a photograph of the piezocatalytic decomposition of the RhB solution in the presence of BFO nanoparticles before and after piezocatalysis. b) Schematic of the BFO nanoparticles-mediated piezocatalytic effect. c) Observed rate constant of RhB degradation with and without free radical scavengers. d) Removal efficiency of various dyes and pharmaceuticals using BFO nanoparticles.

2.2. Synergistically Catalytic Activities through the Piezo-Photocatalytic Effect

UV-vis diffuse reflectance spectroscopy (DRS) was carried out to examine the light absorption properties of the as-prepared BFO NPs. **Figure 3**a shows that our BFO nanocatalysts

display strong absorption within the visible region with bandgap value of 2.29 eV, which is lower than the bandgap values reported for single crystals or thin films.[30] The photocatalytic process is thus realized when above bandgap light illumination is used to photogenerate electrons and holes, which in turn will promote the photodegradation of organic species when reaching the surface of the photocatalytic particles.[23] Combining both light and ultrasonic excitations favors the redox reactions because the additional photogenerated e^- and h^+ will further contribute to the process as they are separated by the mechanically-formed fluctuating piezopotential. The number of photogenerated carriers is significantly higher than that of the thermally generated ones, which enhances the catalytic process (Figure S7, Supporting Information). Given the diffusion length of the charge carriers in BFO,[6, 31] it is likely that this combined process is optimized in below 100 nm size particles. Therefore, the piezo-photocatalytic performance of BFO is exploited under natural sunlight in conjunction with ultrasonication for the degradation of RhB. Figure 3b reveals that the degradation ratio of RhB reaches ~ 54.06% within 10 min of illumination. When the sunlight is combined with the ultrasonic wave, the RhB dye is completely decomposed to reach 100% within 5 min.

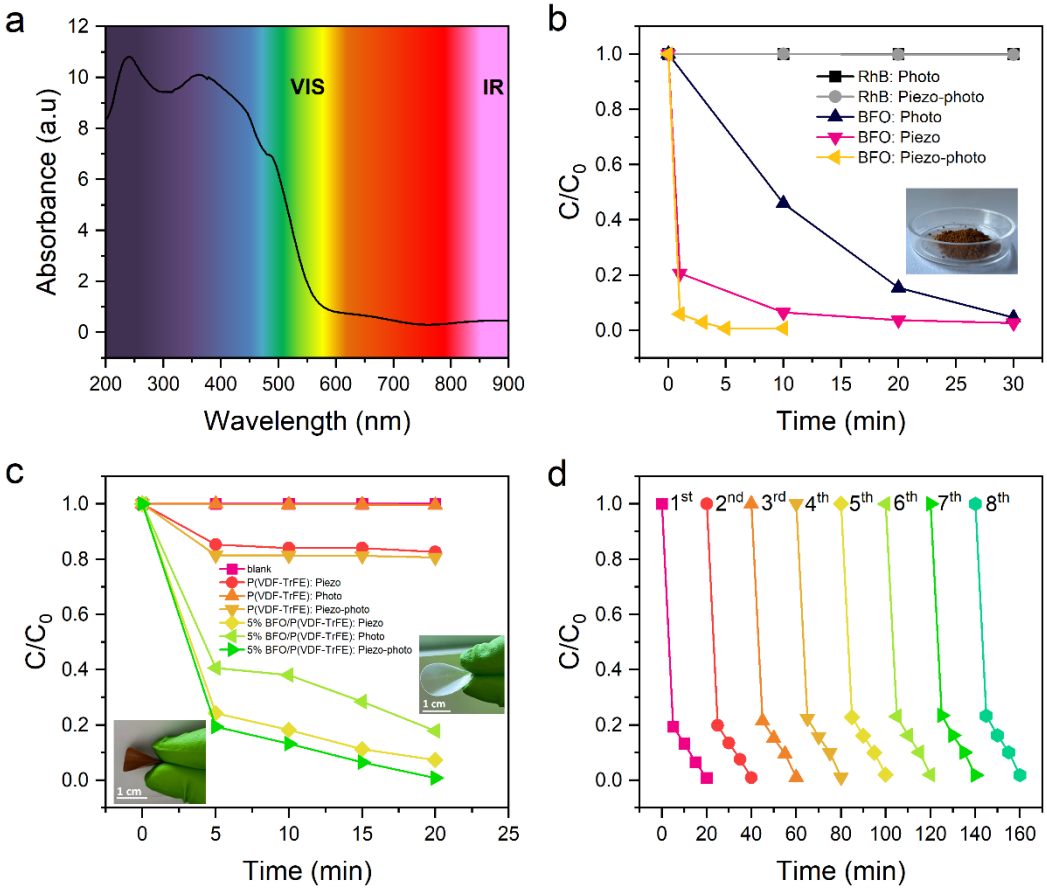

Figure 3. Piezo-photocatalytic performances of $BiFeO_3$ nanoparticles. a) UV-vis absorption spectrum of BiFeO3 nanoparticles. Time-dependent piezo, photo and piezo-photocatalytic degradation efficiency

of RhB using b) BFO nanoparticles and c) the BFO/P(VDF-TrFE) device. d) Cycling performance for BFO/P(VDF-TrFE) by synergistic piezo-photocatalysis.

Under both ultrasonic and sunlight stimulus, the k_{obs} is found to be 0.4175 min^{-1}, which is about 4 times higher than the individual photocatalytic k_{obs} value (0.1035 min^{-1}) and also the fastest piezo-photodegradation rate, to the best of our knowledge (see Table S1, Supporting Information and Figure 4). To consider the amount of pollutant and permit a better comparison, the specific rate constant *k* was further calculated by $\frac{k_{obs}}{[M]}$ with [M] being the concentration of RhB dye. The piezo-photocatalytic rate constant is thus calculated to be 41750 L mol^{-1} min^{-1}, which is the highest degradation rate among the reported values.[11b, 32] The *k*-value for the degradation of RhB using our BFO NPs is 13810 and 10350 L mol^{-1} min^{-1} through piezocatalysis (i.e., with ultrasonication) and photocatalysis (i.e., under light irradiation only), respectively. Thus, the degradation rate via piezo-photocatalysis is observed to be more than 3-fold and 4-fold higher than that via respective piezocatalysis and photocatalysis. This catalytic enhancement underlines the synergy between the photocatalytic and piezocatalytic mechanisms that couple through the piezo-photocatalytic effect.

We demonstrated that the as-prepared BFO NPs are very efficient piezo-photo-catalysts, we now investigate their response when considering $BiFeO_3$/P(VDF-TrFE) composite films in order to tackle issues such as recycling of the catalyst, eliminating, or at least restricting, possible secondary pollution, and increasing the practicality in water treatment applications. UV-vis absorption spectra are displayed in Supporting Information, Figure S11. A control experiment (blank in Figure 3c) has been conducted in the same conditions and no apparent diminution of absorbance is noticed. The characteristics absorbance peak of RhB when using the composite decreased as the illumination/ultrasonication time increased, and approached zero after 20 min (Figure S11, Supporting Information), indicating the degradation of RhB molecules. Note that P(VDF-TrFE) is transparent (bandgap of 5.6 eV) [33] and hence there is no detectable photocatalytic activity under sunlight exposure (Figure 3c, orange upward triangles; Figure S12a, Supporting Information) but, as expected (piezoelectric coefficient of -16 pm V^{-1}), shows a weak piezocatalytic response with about 18% piezo-degradation of RhB after 20 min (Figure 3c, pink circles; Figure S12b, Supporting Information). When considering BFO/P(VDF-TrFE), the degradation ratio of RhB produced by photocatalysis and piezocatalysis are 82 and 92%, respectively (Figure 3c, green leftward triangles and yellow diamonds, respectively and Figure S11a,b, Supporting Information). The piezocatalytic activity of the live video for the flexible BFO/P(VDF-TrFE) catalysts is shown in Supporting

Information (see Figure S13, Supporting Information). The visual (Video S1, Supporting Information) display evidences that the useful catalysts with an ultra-high degradation activity were performed in the dark without applying any external lighting source, which is opening up a new solution for water treatment. In practical scenarios, the piezocatalytic films could be adhered onto a dam, which could perform routine water purification upon the strikes of waves. Interestingly, a remarkable increase of catalytic activity of BFO/P(VDF-TrFE) is found through the synergistic piezo-photocatalytic process (i.e., the piezophototronic effect) allowing to completely decompose RhB dye within 20 min (Figure 3c, green rightward triangles), as further illustrated in Figure S11c (Supporting Information). The observed rate constant of this reaction is 0.2152 min^{-1} (Figure S14, Supporting Information), and an ultra-high degradation rate of RhB dye reaches 21520 L mol^{-1} min^{-1} and makes these BFO/P(VDF-TrFE) films suitable for water cleaning applications. To further exploit the performances of such BFO-based composite catalysts, eight consecutive cycles under a total of 160 min of simultaneous light and ultrasonic wave are conducted and show that the superior RhB degradation rate of BFO/P(VDF-TrFE) can be well maintained (Figure 3d and Figure S15, Supporting Information), indicating the high reuse stability of the catalyst. XRD and Raman characterizations (Figure S16, Supporting Information) of the sample after the cycling tests shows that the piezo-photocatalytic process does not reveal any significant change in the crystalline structure of BFO/P(VDF-TrFE), implying their good durability. The excellent reuse stability, recyclability with ultra-high degradation activity endows the as-prepared multicatalytic BFO/P(VDF-TrFE) system great potential in practical wastewater treatment, and possibly in other applications such as water splitting for hydrogen production.

Finally, the $BiFeO_3$ NPs and $BiFeO_3$/P(VDF-TrFE) photo-, piezo-, and piezo-photocatalytic responses are gathered in Figure 4 together with other currently reported photo- and piezoelectric catalysts (Table S1, Supporting Information). A direct comparison of the properties of the materials (such as their piezoelectric coefficient and dielectric constant) is not straightforward (Table S3, Supporting Information). Indeed, the reported piezoelectric coefficients most often correspond to the bulk values, which are overestimated especially when going towards nanoscale, where the polar distortion drastically drops down making the material less non-centrosymmetric, i.e., less piezoelectric.[18] Note that BFO is a rather special ferroelectric material, where both polar displacements and oxygen octahedral tilts coexist, in contrast to $BaTiO_3$, $KNbO_3$, PZT and many others. These oxygen tilts are an extra degree of freedom, allowing to relax the structure when subjected to external constraints while keeping the polar distortion and thus the polarization.[34] In case of NPs, the surface somehow imposes

a pressure, which in classical ferroelectrics tends to reduce the polar distortions,[35] while in case of BFO it is believed that the oxygen tilts release the surface pressure and allow BFO NPs to keep its bulk-like polarization state. Furthermore, the considered dielectric constant often corresponds to different measurement frequencies, making the comparison difficult. Nonetheless, when trying to compare the piezocatalytic and piezo-photocatalytic performances under similar experimental conditions, one can see our synthesized materials show significantly greater efficiencies than those reported in the literature for any other compounds making them promising candidates for the degradation of organic pollutants. This opens a path towards other applications in energy harvesting and production, biological research and medicine with for instance chemo-catalytic tumor therapy.

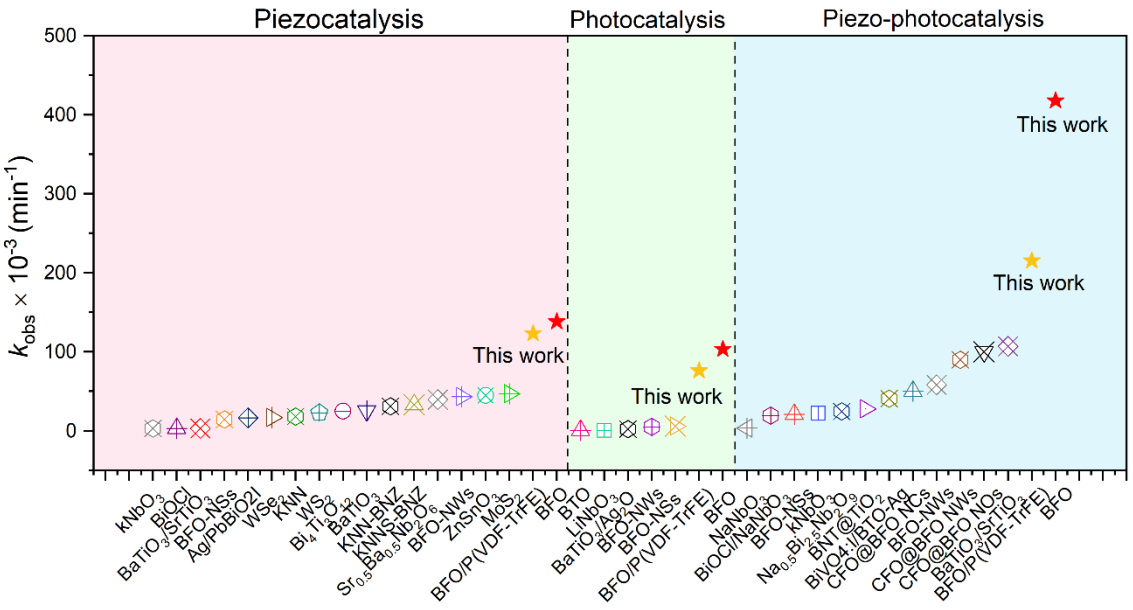

Figure 4. Degradation rate constant k_{obs} for various materials. BFO (red stars) and BFO/P(VDF-TrFE) (orange stars) piezo, photo and piezo-photocatalytic activities compared with other ferro/piezoelectric materials (see the details in Supporting Information Table S1).

3. Conclusion

In summary, we have shown that 60 nm size BFO NPs display a giant piezocatalytic effect with record values of degradation rates. Through the synergistic piezo-photocatalytic process, BFO nanocatalysts achieve a full degradation efficiency for decomposing the model Rhodamine B dye, corresponding to a kinetic rate constant of 41750 L mol^{-1} min^{-1}. Moreover, BFO NPs display a wide piezocatalytic versatility allowing to efficiently piezo-degrade various dyes and antibiotics. These remarkable piezocatalytic and piezo-photocatalytic effects are explained by the concomitant presence of a high piezoelectric response (which is kept despite the nanosize),

a low dielectric constant, and a low bandgap. Furthermore, the nanosize of the particles is limiting the detrimental charge carrier recombination, not to mention the increase of the surface-to-volume ratio. Moreover, to increase the practicability of those BFO NPs, BFO/P(VDF-TrFE) composite films were designed. These flexible films keep excellent piezocatalytic and piezo-photocatalytic performances, are stable and reusable, and thus provide a valuable solution for wastewater treatment in practical scenarios. These findings make BFO a very promising catalysts and open the path towards more research activities and various applications such as hydrogen and methane generation or cancer therapy, e.g., chemo-piezocatalytic or sonodynamic therapies, where ultrasound-triggered piezoelectric reactive oxygen species (ROS) generation are required. They should also encourage various material science communities including optoelectronic, energy and energy harvesting, environment, or biology to further explore such nanoscale ferroelectric materials.

4. Experimental Section

Synthesis of $BiFeO_3$ Nanoparticles: $BiFeO_3$ NPs were synthesized from a chemical bath containing a stoichiometric amount of bismuth nitrate pentahydrate ($Bi(NO_3)_3.5H_2O$, 98% Alfa Aesar) and iron nitrate nonahydrate ($Fe(NO_3)_3.9H_2O$, 98-101% Alfa Aesar), as previously reported.[1, 23] Ammonia was used as chelating agent for complexation with bismuth and ferrite nitrates. This mixture was then magnetically stirred for 2 h at 50 °C in oil bath, resulting in the precipitation of BFO NPs followed by annealing the as-obtained product at 500 °C for 2 h in air.

Fabrication of $BiFeO_3$ (BFO)/P(VDF-TrFE) Composite Film: To prepare the BFO/P(VDF-TrFE) (75-25) composite film, 0.39 g of BFO NPs were firstly dispersed in N,N-dimethylformamide (DMF, 12 mL; Merck≥ 99,5%) and sonicated in an ultrasonic bath for 90 min at room temperature. 1.60 g of P(VDF-TrFE) (75-25) (FC25; Arkema Piezotech) was then added into the solution, followed by vigorous mechanical stirring for 2 h at 56 °C. The solution was then cast onto glass plates using a film applicator (Elcometer 4340, United Kingdom). Eventually, the composite thin film was peeled up from the glass plates after drying, and treated at 140 °C for 50 min in a vacuum oven to obtain a higher crystallinity. Pure P(VDF-TrFE) thin films were also synthesized under the same experimental conditions for comparison purposes.

Materials Characterization: X-ray diffraction (XRD, PANalytical Aeris diffractometer) was employed to investigate the structural properties of the prepared materials. The morphology and the size of the BFO NPs were analyzed by using transmission electron microscopy (TEM)

and High-resolution TEM (JEOL JEM 2100) operated at 200 kV. The surface morphology and cross-section of the BFO/P(VDF-TrFE) were analyzed via field-emission scanning electron microscopy (SEM, Thermo Fisher Verios 4G HP). Raman measurements were performed using a LABRAM Horiba-Jobin-Yvan spectrometer under He-Ne laser excitation (632.8 nm). Room-temperature diffuse reflectance spectra of the sample in the ultraviolet-visible (UV-vis) region were recorded in the 200-900 nm wavelength range on a Perkin Elmer spectrometer (Lambda 850) equipped with a Harrick Praying Mantis^{TM} diffuse reflectance accessory using the non-absorbing $BaSO_4$ as a reflectance reference. The macroscopic piezoelectric properties of the films sandwiched with electrodes were measured using a piezoelectric tester (TF-2000, Aixacct) at a frequency of 20 Hz and a magnitude of electric field of 1 MV cm^{-1}. The nanoscale piezoelectric properties were carried out by piezo-force microscopy (PFM) using an atomic force microscope (Cypher, Asylum) for the simultaneous acquisition of in-plane and out-of-plane responses.

Catalytic Experiments: The catalytic performance of the BFO NPs was investigated on the degradation of Rhodamine B (RhB). Typically, 10 mg of BFO NPs was dispersed in 10 mL aqueous RhB solution with a concentration of 10^{-5} M. Before the catalytic reaction, the suspension was stirred in darkness for 30 min to ensure the adsorption-desorption equilibrium. For piezocatalytic experiments, samples were subjected to stress using an ultrasonic source (power and frequency 100 W, 45 kHz) and kept in dark environment to avoid any effect from the light. To verify the role of free radicals, the concentration of the added tert-butyl alcohol (TBA, 99% Alfa Aesar), benzoquinone (BQ, 98% Alfa Aesar) or disodium ethylene diamine tetra-acetate dehydrate (EDTA-2Na, 99% Alfa Aesar) was 1 mM. Photocatalytic experiments were conducted under illumination of natural sunlight (at the zenith in a sunny day i.e., a power of ~1 kW m^{-2}). For the piezo-photocatalytic degradation experiments, natural sunlight was used in combination with the ultrasonic source. At a given interval time, about 3 mL of the solution was picked up through a PVDF syringe filter to remove the catalyst particles. The degradation of RhB was monitored by measuring the absorbance of the filtered solution as a function of time using a Lamda 850 UV-vis spectrometer. The catalytic performance of the BFO/P(VDF-TrFE) composite film was also studied via the degradation of RhB. For this, circular films with a diameter of 2.2 cm were used as catalysts. The rest of the conditions (ultrasonication, dye volume and concentration) were the same as mentioned for the catalytic experiment of BFO NPs.

Micro-pollutants Degradation Induced by the Piezocatalytic Effect: Experiments were performed to study the degradation of various organic pollutants in the presence of our BFO

NPs under the specifications of a 45 kHz ultrasonic wave (100 W) in the dark. The organic pollutants chosen for this study were Methylene Blue, Indigo Carmine, Methyl Orange, Tetracycline and Carbamazepine, each having a concentration of 10^{-5} M. 10 mg of BFO NPs were dispersed in 10 mL of the above solution and subjected to the external mechanical stress in the dark, once the adsorption-desorption equilibrium was reached. To exclude the influence of increasing temperature on piezocatalytic reaction, water was replaced every 15 min in the ultrasonic bath, kept in the dark. The concentration of the organic pollutants was measured at different times using a UV-vis spectrophotometer.

Supporting Information

Supporting Information is available from the Wiley Online Library or from the author.

Acknowledgements

This work was supported by the Tunisian Ministry of Higher Education and Scientific Research (MHESR) and a public grant over-seen by the French National Research Agency (ANR) as part of the "Investissements d'Avenir" program (Reference No. ANR-10-LABX-0035, Labex NanoSaclay), TATOO-ANR-21-CE0-9-0033-02, UFO-ANR-21-CE09-0028-02, PHC Slovenian-French Proteus mobility grant (BI-FR/21-22-PROTEUS-004), Slovenian Research Agency (program P2-0105), ARRS (Slovenian Research agency) J2-2508, and FNR-Luxembourg INTERmobility grant (INTER/Mobility/19/13992074).

Conflict of Interest

The authors declare no conflict of interest.

Author Contributions

W.A. conceived the research idea, designed the experiments and carried out material synthesis and device fabrication. H.M.M., J.K. and B.D. guided and supervised the work. M.O. performed TEM and SEM measurements. W.A. conducted the piezo/photocatalytic experiments and realized the necessary characterizations. Macroscopic piezoelectric measurements were carried out by M.F. V.G. and S.F. performed and analyzed the PFM experiments. W.A. analyzed the data and wrote the manuscript, with input from B.D. All authors discussed the results and commented on the manuscript.

Received: ((will be filled in by the editorial staff))
Revised: ((will be filled in by the editorial staff))
Published online: ((will be filled in by the editorial staff))

References

[1] W. Amdouni, M. Otoničar, P. Gemeiner, V. Butin, N. Guiblin, H. Maghraoui-Meherzi, B. Dkhil, *Angew. Chem. Int. Ed* **2023**, 62, e202215700.

[2] S. Irfan, S. Rizwan, Y. Shen, L. Li, Asfandiyar, S. Butt, C. W. Nan, *Sci Rep* **2017**, 7, 42493.

[3] a) F. Mushtaq, X. Chen, S. Staufert, H. Torlakcik, X. Wang, M. Hoop, A. Gerber, X. Li, J. Cai, B. J. Nelson, S. Pané, *J. Mater. Chem. A* **2019**, 7, 24847; b) M. Yan, Y. Wu, Y. Yan, X. Yan, F. Zhu, Y. Hua, W. Shi, *ACS Sustain. Chem. Eng.* **2015**, 4, 757.

[4] C. Foo, Y. Li, K. Lebedev, T. Chen, S. Day, C. Tang, S. C. E. Tsang, *Nat Commun* **2021**, 12, 661.

[5] a) J. Xue, S. Ma, Y. Zhou, Z. Zhang, M. He, *ACS Appl. Mater. Interfaces* **2015**, 7, 9630; b) H. Khan, M. G. Rigamonti, D. C. Boffito, *Appl. Catal. B: Environ* **2019**, 252, 77.

[6] C. Paillard, X. Bai, I. C. Infante, M. Guennou, G. Geneste, M. Alexe, J. Kreisel, B. Dkhil, *Adv Mater* **2016**, 28, 5153.

[7] L. Su, L. Zou, C. C. Fong, W. L. Wong, F. Wei, K. Y. Wong, R. S. Wu, M. Yang, *Biosens. Bioelectron* **2013**, 46, 155.

[8] Y. Sugawara, K. Onitsuka, S. Yoshikawa, Q. Xu, R. E. Newnham, K. Uchino, *J. Am. Ceram. Soc* **1992**, 75, 996.

[9] a) S. Tu, Y. Guo, Y. Zhang, C. Hu, T. Zhang, T. Ma, H. Huang, *Adv. Funct. Mater* **2020**, 30, 2005158; b) X. Zhou, B. Shen, A. Lyubartsev, J. Zhai, N. Hedin, *Nano Energy* **2022**, 96; c) L. Lu, N. Liang, H. Sun, Q. Zhang, X. Hao, *J. Mater* **2022**, 8, 47.

[10] Y. Feng, L. Ling, Y. Wang, Z. Xu, F. Cao, H. Li, Z. Bian, *Nano Energy* **2017**, 40, 481.

[11] a) J. Wu, Q. Xu, E. Lin, B. Yuan, N. Qin, S. K. Thatikonda, D. Bao, *ACS. Appl. Mater. Interfaces* **2018**, 10, 17842; b) S. Xu, Z. Liu, M. Zhang, L. Guo, *J. Alloys Compd* **2019**, 801, 483; c) D. Liu, C. Jin, F. Shan, J. He, F. Wang, *ACS. Appl. Mater. Interfaces* **2020**, 12, 17443.

[12] D. Yu, Z. Liu, J. Zhang, S. Li, Z. Zhao, L. Zhu, W. Liu, Y. Lin, H. Liu, Z. Zhang, *Nano Energy* **2019**, 58, 695.

[13] S. Singh, N. Khare, *Nano Energy* **2017**, 38, 335.

[14] B. Yuan, J. Wu, N. Qin, E. Lin, Z. Kang, D. Bao, *Appl. Mater. Today* **2019**, 17, 183.

[15] X. Xu, X. Lin, F. Yang, S. Huang, X. Cheng, *J. Phys. Chem. C* **2020**, 124, 24126.

[16] J. Dai, N. Shao, S. Zhang, Z. Zhao, Y. Long, S. Zhao, S. Li, C. Zhao, Z. Zhang, W. Liu, *ACS Appl. Mater. Interfaces* **2021**, 13, 7259.

[17] S. Priya, H.-C. Song, Y. Zhou, R. Varghese, A. Chopra, S.-G. Kim, I. Kanno, L. Wu, D. S. Ha, J. Ryu, R. G. Polcawich, *Energy. Harvest. Syst* **2019**, 4, 3.

[18] a) Y. Huan, X. Wang, J. Fang, L. Li, *J. Eur. Ceram. Soc* **2014**, 34, 1445; b) C. A. Randall, N. Kim, J.-P. Kucera, W. Cao, T. R. Shrout, *J. Am. Ceram. Soc* **1998**, 81, 677; c) M. Muthuramalingam, D. E. Jain Ruth, M. Veera Gajendra Babu, N. Ponpandian, D. Mangalaraj, B. Sundarakannan, *Scr. Mater* **2016**, 112, 58; d) R. Pramanik, M. K. Sahukar, Y. Mohan, B. Praveenkumar, S. R. Sangawar, A. Arockiarajan, *Ceram. Int* **2019**, 45, 5731.

[19] a) D. Lebeugle, D. Colson, A. Forget, M. Viret, *Appl. Phys. Lett.* **2007**, 91, 022907 ; b) Z. W. Wu, Q. Sun, K. Ding, C. X. Gu, *J. Phys. D: Appl. Phys.* **2005**, 38, 4296.

[20] S. Skiadopoulou, V. Goian, C. Kadlec, F. Kadlec, X. F. Bai, I. C. Infante, B. Dkhil, C. Adamo, D. G. Schlom, S. Kamba, *Phy. Rev. B* **2015**, 91, 174108.

[21] a) F. Mushtaq, X. Chen, M. Hoop, H. Torlakcik, E. Pellicer, J. Sort, C. Gattinoni, B. J. Nelson, S. Pane, *iScience* **2018**, 4, 236; b) H. You, Z. Wu, L. Zhang, Y. Ying, Y. Liu, L. Fei, X. Chen, Y. Jia, Y. Wang, F. Wang, S. Ju, J. Qiao, C. H. Lam, H. Huang, *Angew. Chem. Int. Ed* **2019**, 58, 11779; c) Y.-L. Liu, J. M. Wu, *Nano Energy* **2019**, 56, 74; d)F. Mushtaq, X. Chen, H. Torlakcik, B. J. Nelson, S. Pané, *Nano Res* **2020**, 13, 2183.

[22] C. Paillard, G. Geneste, B. L., J. Kreisel, M. Alexe, B. Dkhil, in *Emerging Photovoltaic Materials: Silicon & Beyond*, Wiley Online Library 2018.

[23] W. Amdouni, L. Yedra, M. Otoničar, P. Gemeiner, B. Dkhil, H. Maghraoui-Meherzi, *J. Mater. Sci* **2022**, 57, 18726.

[24] M. Fricaudet, K. Žiberna, S. Salmanov, J. Kreisel, D. He, B. Dkhil, T. Rojac, M. Otoničar, P.-E. Janolin, A. Bradeško, *ACS Appl. Electron. Mater* **2022**, 4, 5429.

[25] a) L. Liu, T. Rojac, J. Kimpton, J. Walker, M. Makarovic, J.-F. Li, J. Daniels, *Appl. Phys. Lett* **2020**, 116, 122901; b) A. Tuluk, T. Mahon, S. Van der Zwaag, P. Groen, *J. Alloys. Compd* **2021**, 868, 159186.

[26] M. Hammer, M. J. Hoffmann, *J. Am. Ceram. Soc* **1998**, 81, 3277.

[27] J. Wu, Q. Xu, E. Lin, B. Yuan, N. Qin, S. K. Thatikonda, D. Bao, *ACS Appl. Mater. Interfaces* **2018**, 10, 17842.

[28] X. Zhou, S. Wu, C. Li, F. Yan, H. Bai, B. Shen, H. Zeng, J. Zhai, *Nano Energy* **2019**, 66.

[29] Z. Xie, X. Tang, J. Shi, Y. Wang, G.-L. Yuan, J.-M. Liu, *Nano Energy* **2022**, 98.

[30] M. O. Ramirez, A. Kumar, S. A. Denev, N. J. Podraza, X. S. Xu, R. C. Rai, Y. H. Chu, J. Seidel, L. W. Martin, S.-Y. Yang, Y. Yang, E. Saiz, J. F. Ihlefeld, S. Lee, J. Klug, S. W. Cheong, M. J. Bedzyk, O. Auciello, D. G. Schlom, R. Ramesh, J. Orenstein, J. L. Musfeldt, V. Gopalan, *Phys. Rev. B* **2009**, 79, 224106.

[31] J. E. Spanier, V. M. Fridkin, A. M. Rappe, A. R. Akbashev, A. Polemi, Y. Qi, Z. Gu, S. M. Young, C. J. Hawley, D. Imbrenda, G. Xiao, A. L. Bennett-Jackson, C. L. Johnson, *Nat. Photon* **2016**, 10, 611.

[32] a) S. Thangavel, P. Pazhamalai, K. Krishnamoorthy, Y. Sivalingam, D. Arulappan, V. Mohan, S. J. Kim, G. Venugopal, *Chemosphere* **2022**, 292, 133398; b) L. Li, Y. Ma, G. Chen, J. Wang, C. Wang, *Scr. Mater.* **2022**, 206; c) X. Liu, L. Xiao, Y. Zhang, H. Sun, *J. Materiomics* **2020**, 6, 256.

[33] D. Mandal, K. Henkel, K. Müller, D. Schmeißer, *Bull. Mater. Sci* **2010**, 33, 457.

[34] a) I. C. Infante, S. Lisenkov, B. Dupe, M. Bibes, S. Fusil, E. Jacquet, G. Geneste, S. Petit, A. Courtial, J. Juraszek, L. Bellaiche, A. Barthelemy, B. Dkhil, *Phys. Rev. Lett* **2010**, 105, 057601; b) A. J. Hatt, N. A. Spaldin, C. Ederer, *Phys. Rev. B* **2010**, 81, 054109; c) D. Sando, A. Agbelele, C. Daumont, D. Rahmedov, W. Ren, I. C. Infante, S. Lisenkov, S. Prosandeev, S. Fusil, E. Jacquet, C. Carretero, S. Petit, M. Cazayous, J. Juraszek, J. M. Le Breton, L. Bellaiche, B. Dkhil, A. Barthelemy, M. Bibes, *Phil. Trans. R. Soc. A* **2014**, 372, 20120438.

[35] A. K. Sood, N. Chandrabhas, D. V. Muthu, A. Jayaraman, *Phys. Rev. B* **1995**, 51, 8892.

The Table of contents

Highly efficient and versatile $BiFeO_3$ nanoparticle piezocatalysts are found to exhibit strong piezocatalytic and synergistic piezo-photocatalytic effects (100% degradation ratio of Rhodamine B within 5 min), and are embedded into a P(VDF-TrFE) polymer to design flexible, stable and reusable multicatalytic system for wastewater treatment using mechanical forces and sunlight.

Wafa Amdouni, Matthieu Fricaudet, Mojca Otoničar, Vincent Garcia, Stephane Fusil, Jens Kreisel, Hager Maghraoui-Meherzi, and Brahim Dkhil**

$BiFeO_3$ Nanoparticles: The "Holy-Grail" of Piezo-photo-catalysts?